ACS APPLIED MATERIALS & INTERFACES

Research Article

www.acsami.org

Highly Efficient Low-Bandgap Polymer Solar Cells with Solution-Processed and Annealing-Free Phosphomolybdic Acid as Hole-Transport Layers

Xu Jia,[†] Liang Shen,*[,†] Mengnan Yao,[‡] Yan Liu,[§] Wenjuan Yu,[†] Wenbin Guo,[‡] and Shengping Ruan*[,‡]

[†]State Key Laboratory on Integrated Optoelectronics, [‡]College of Electronic Science and Engineering, and [§]Key Laboratory of Bionic Engineering (Ministry of Education), Jilin University, Changchun 130012, People's Republic of China

ABSTRACT: We demonstrate a novel solution-processed method to fabricate a stable anode buffer layer without any annealing process. As we know, buffer layers in polymer solar cells (PSCs) are always prepared by the traditional high-vacuum thermal evaporation or annealing-treated spin-coating methods, but the fabricating processes are complicated and time-consuming. Here, a solution method without any annealing to fabricate phosphomolybdic acid (PMA) as anode buffers is presented, which brings an obvious improvement of power conversion efficiency (PCE) from 1.75% to 6.57% by optimizing the PMA concentrations and interface pretreatment with device structure shown as ITO/TiO_2/PCDTBT:$PC_{70}BM$/PMA/Ag. The improvement is ascribed to the fine energy-level matching and perfect surface modification. This annealing-free method greatly simplifies the device fabrication process and supplies a wide way to achieve a large area fabrication for PSCs.

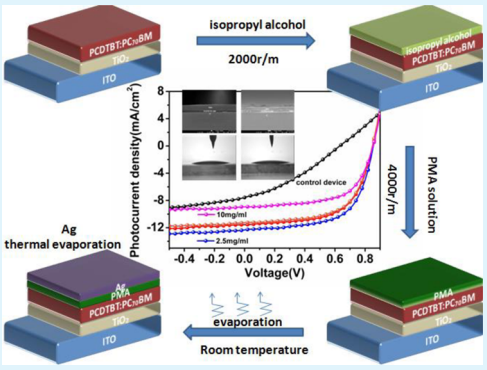

KEYWORDS: *phosphomolybdic acid, isopropyl alcohol, PCDTBT, polymer solar cell*

INTRODUCTION

Bulk heterojunction (BHJ) polymer solar cells (PSCs) are a promising candidate for next-generation low-cost energy-conversion devices with the advantages of low cost, flexibility, and large-area fabrication features.[1−5] Great efforts have been made in recent years to improve the performance of PSCs. Recent advances in the design and synthesis of new polymer materials combined with microstructural engineering of the photoactive layers have led to the development of PSCs with power conversion efficiency (PCE) breaking through 10%.[6−10] In addition to active materials, the effects of interfacial layers inserted between active layers and electrodes have also been studied extensively, and their key role on the charge transport has been demonstrated.[11−16]An ideal interlayer system should contain four basic characteristics: (1) easy to process at room temperature on large-area substrates; (2) highly transparent from ultraviolet to near-infrared wavelengths of the solar spectra;[17−19] (3) having appropriate energy levels to mediate the energy mismatch between active layer and electrodes; and (4) ability to block minority carrier flow toward the inappropriate electrodes. These interlayer materials characteristics have indeed been found to have a profound influence on device performance.[20−24] The ideal interlayer material system should satisfy all or most of the above requirements.

Among the hole-transport layers (HTLs), poly(3,4-ethylenedioxythiophene): polystyrenesulfonate (PEDOT:PSS) is widely used for its relatively good optical transparency (80−87%), deep work function (−5.1 eV), tunable range of conductivity, and its facility to form continuous thin film. Apart from all these favorable features, researchers find PEDOT:PSS reacts with organic active layers[25−28] because of its acidic and hygroscopic nature, which will degrade the environmental stability of device in turn. Much work has been done to search for the substitution of PEDOT:PSS. To date the most favorable substitutes of PEDOT:PSS are the transition metal oxides, including WO_3,[29−31] MoO_3,[32−35] and V_2O_5,[36−38] which can improve both PCE and lifetime of PSCs. Generally, the transition metal oxides are deposited on the device in two ways, vacuum deposition and solution-based spin-coating. However, vacuum deposition process is both energy-consuming and time-consuming, which make it more expensive than wet-chemical processing with printing techniques, unless the throughput is high enough, which is achievable with roll-to-roll production for both vacuum and solution-based processing. For solution-based spin-coating, it always requires a post-annealing process combined with high temperature to strengthen uniform film by evaporating the solvent, which will destroy surface morphology and degrade the polymer. To resolve all the problems, in this paper, solution-processed annealing-free phosphomolybdic acid (PMA) was used as HTL to fabricate inverted PSCs. PMA is a type of stable, commercially available, and cost-effective soluble oxide cluster with desirable features, including excellent thermal stability, highly tunable structural properties, high transparency in the visible spectrum, and good solubility in many polar solvents.[39,40] Here, the PMA powder was dissolved in isopropyl

Received: December 14, 2014
Accepted: February 19, 2015
Published: February 19, 2015

DOI: 10.1021/am508828n
ACS Appl. Mater. Interfaces 2015, 7, 5367−5372

alcohol (IPA) and then spin-coated on top of the active layer without any postannealing to form a thin HTL, which brings an obvious improvement of PCE from 1.75% to 6.57% by optimizing the IPA pretreatment and PMA concentrations. In 2014, Zhu et al.[39] demonstrate a cost-effective commercial soluble organic solar cell using PMA as HTL in poly[[4,8-bis[(2-ethylhexyl)oxy]benzo[1,2-b:4,5-b0]dithiophene-2,6-diyl][3-fluoro-2-[(2-ethylhexl)carbonyl]thieno[3,4-*b*]-thiophenediyl]] (PTB7) mixed with [6,6]-phenyl-C_{71}-butyric acid methyl ester ($PC_{70}BM$) systems. In our work, blend of poly[*N*-9″-hepta-decanyl-2,7-carbazole-*alt*-5,5-(4′,7′-di-2-thienyl-2′,1′,3′-benzothiadiazole) (PCDTBT):[6,6]-phenyl C_{71}-butyric acid methyl ester ($PC_{70}BM$) was selected as the active layer, and the commonly used TiO_2 was chosen as the electron transport layer (ETL). In addition, an IPA-pretreatment procedure was applied before spin-coating IPA-soluted PMA to further decrease the contact angle and smooth the interfaces, which results in an improvement in the performance of device. Our work extends the application of PMA as HTL in different systems of active layer. The solution-processed annealing-free method improves the device performance and simplifies fabrication process simultaneously.

EXPERIMENTAL SECTION

The fabrication process of PSCs are shown schematically in Figure 1. The indium tin oxide (ITO) coated glass substrates(a sheet resistance

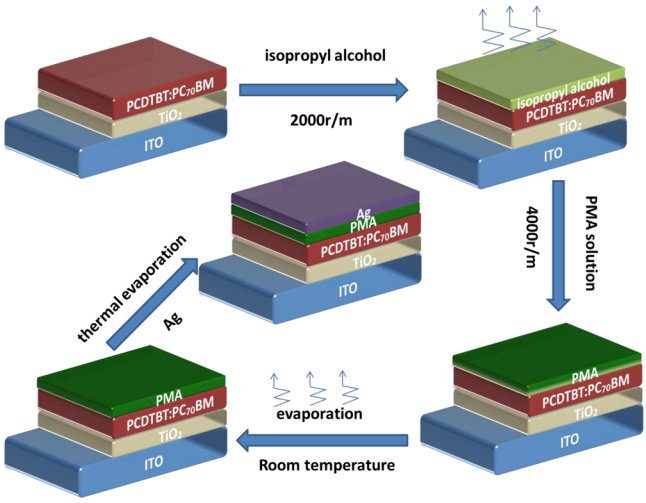

Figure 1. Fabrication process of PSCs.

of 15Ω/sq) were precleaned by acetone, ethanol, and deionized water, successively, and then dried by nitrogen flow. Anatase TiO_2 thin films were prepared as described in our previous papers[41,42] to act as ETL. PCDTBT (Lumtec Corp, used as received) blending with $PC_{70}BM$ (Lumtec Corp, used as received) in 1:4 weight ratio was dissolved in 1,2-dichlorobenzene to produce 7 mg/mL solution. The blend was stirred for 72 h in glovebox filled with argon. The PCDTBT:$PC_{70}BM$ active layer was prepared by spin coating on top of TiO_2 film surface and annealing at 70 °C for 25 min in glovebox. The PMA powder was dissolved in IPA and stirred overnight with different concentrations (1, 2.5, 5, and 20 mg/mL). All PMA solutions were spun at 4000 rpm for 30 s without any postannealing process. Finally, a 100 nm Ag layer was thermally deposited under a high vacuum (5×10^{-4} Pa) through a shadow mask to function as anodes. The deposition rate was ∼0.2 nm/s, which was monitored with a quartz-oscillating thickness monitor (ULVAC, CRTM-9000). The active area of the device was ∼0.06 cm^2. A Hitachi S-4500 scanning electron microscope (SEM) operated at an accelerating voltage of 15 kV was used to observe the cross section and estimate the thickness of each layer in the device. UV-1700 was used to characterize the absorption ability of PMA layer in the wavelength range from 300 to 1000 nm. Electrochemical measurement of PMA was performed with a Bioanalytical Systems BAS10B/Welectrochemical workstation. The current−voltage (*J*−*V*) characteristics were measured with a computer-programmed Keithley 2601 source meter under AM1.5G solar illumination with an Oriel 300 W solar simulator intensity of 100 mW/cm^2. The light intensity was measured with a photometer (International Light, IL1400), which was corrected by a standard silicon solar cell. The incident-photon-to-current efficiency conversion (IPCE) spectra for the cells were measured with Crowntech QTest Station 1000AD. Impedance spectroscopy, which measures the dielectric properties of a material and interface as the function of frequency, was measured by an impedance analyzer (Wayne Kerr Electronics 6520B) with a bias of 1 V in the frequency range of 20 Hz−1 MHz.

RESULTS AND DISCUSSION

First, we characterized the absorption spectrum of PMA film with the wavelength range from 300 to 1000 nm, as shown in Figure 2a. The PMA film shows a high transmittance in the

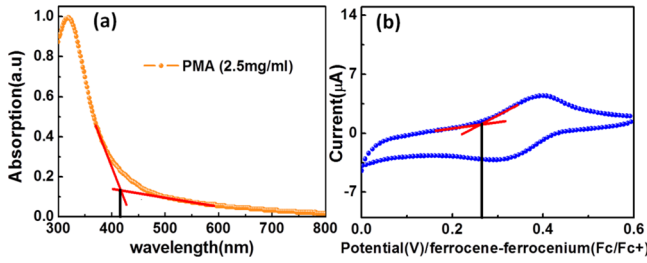

Figure 2. (a) The absorption spectrum of PMA film with the wavelength range from 300 to 1000 nm. (b) The cyclic voltammetry measurements of PMA in dichloromethane.

wavelength range of more than 500 nm, which lowers the absorption competition with the active layer. The absorption onset of PMA film is 416 nm, which indicates the optical bandgap of PMA is ∼2.98 eV. As shown in Figure 2b, the cyclic voltammetry measurements of PMA in dichloromethane were performed to estimate the position of the frontier orbital levels with a reference electrode of ferrocene−ferrocenium (Fc/Fc+). Clearly, PMA has a reversible process in the positive scanning range. From the onset of the reversible oxidation peaks, it can be found that the onset oxidation potential (E_{ox}) is 0.26 V for PMA. A corresponding top of valence band of −4.72 eV for PMA is obtained when ferrocene−ferrocenium (4.46 eV) is used as the reference electrode, which is higher than the highest occupied molecular orbital (HOMO) level of PCDTBT (−5.5 eV). The detailed energy level diagrams of each layer material are shown in Figure 3. It is observed that the energy matching between PMA and PCDTBT reveals that the PMA can transport holes from active layer to the Ag electrode. At the same time, the bottom of the conduction band of PMA is −1.74 eV, much higher than the lowest unoccupied molecular orbital (LUMO) level of PCDTBT (−3.6 eV). In this case, the PMA layer not only works as the HTL, but it also blocks the electrons. Therefore, the PMA could prevent the charge carriers recombination at active layer/Ag electrode interface effectively. *J*−*V* characterization of devices with 2.5 and 5 mg/mL PMA were performed, and the results were shown in Figure 4. Each of the two curves was S-shaped, which led to a terrible performance of devices. The fill factor (FF) of devices based on 2.5 and 5 mg/mL PMA are no more than 22%, and almost no

DOI: 10.1021/am508828n
ACS Appl. Mater. Interfaces 2015, 7, 5367−5372

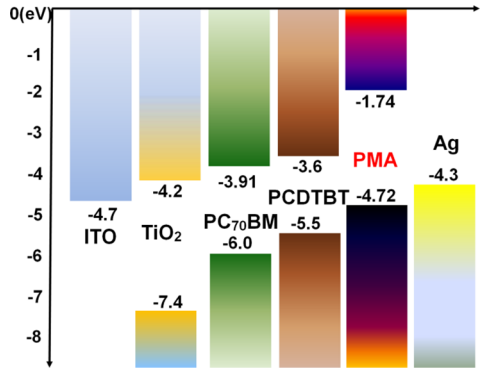

Figure 3. Detailed energy-level diagrams of each layer material.

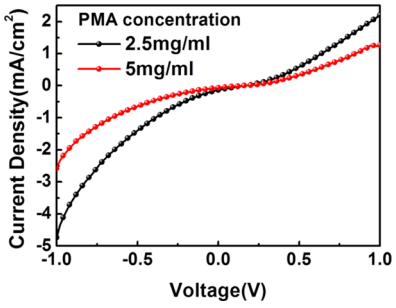

Figure 4. *J*–*V* characterization of devices with 2.5 and 5 mg/mL PMA with device structure of ITO/TiO_2/PCDTBT:$PC_{70}BM$/PMA/Ag tested under AM1.5G solar illuminations.

power conversion efficiency (PCE) is observed. S-curves in bulk heterojunction photovoltaic are caused by the extraction of charges near the electrode. Such factors could include surface recombination, partially blocking contacts caused by interfacial layers. In our work, the S-curves occur for the reason that the contact is not good enough when the PMA solution is directly deposited on active layer, as evidenced in the SEM image of Figure 5a. The fluctuations of the PMA layer result in much more inhomogeneous surface potential and larger series resistance. The holes can not be extracted effectively and thus accumulate at the interface of active layer.

To resolve this problem, a surface pretreatment method, which is spin-coating a layer of IPA on top of active layer before covering the PMA layer, is performed. To see clearly the interface changes, the PMA layers were spin-coated at a fixed speed of 1000 r/min to obtain a thicker film. As shown in Figure 5a,b, the surface of active layer is much smoother, and the area boundaries between active layer and PMA layer are almost indistinguishable. This means that the surface pretreatment with IPA can improve the contact between active layer and PMA layer. To further confirm the effect of the pretreatment by IPA, we measured the contact angle of the PMA solution on the surface of active layer. As shown Figure 5c, the average contact angle of PMA solution on bare active layer before surface modification was measured to be 17.2°, while the average contact angle reduced to 13.1° upon treatment with neat IPA, as evidenced in Figure 5d. As we know, high contact angle makes it difficult to deposit a solution on top of another layer by spin coating. The reduced contact angle enhances the spreading of the solution. It is beneficial to

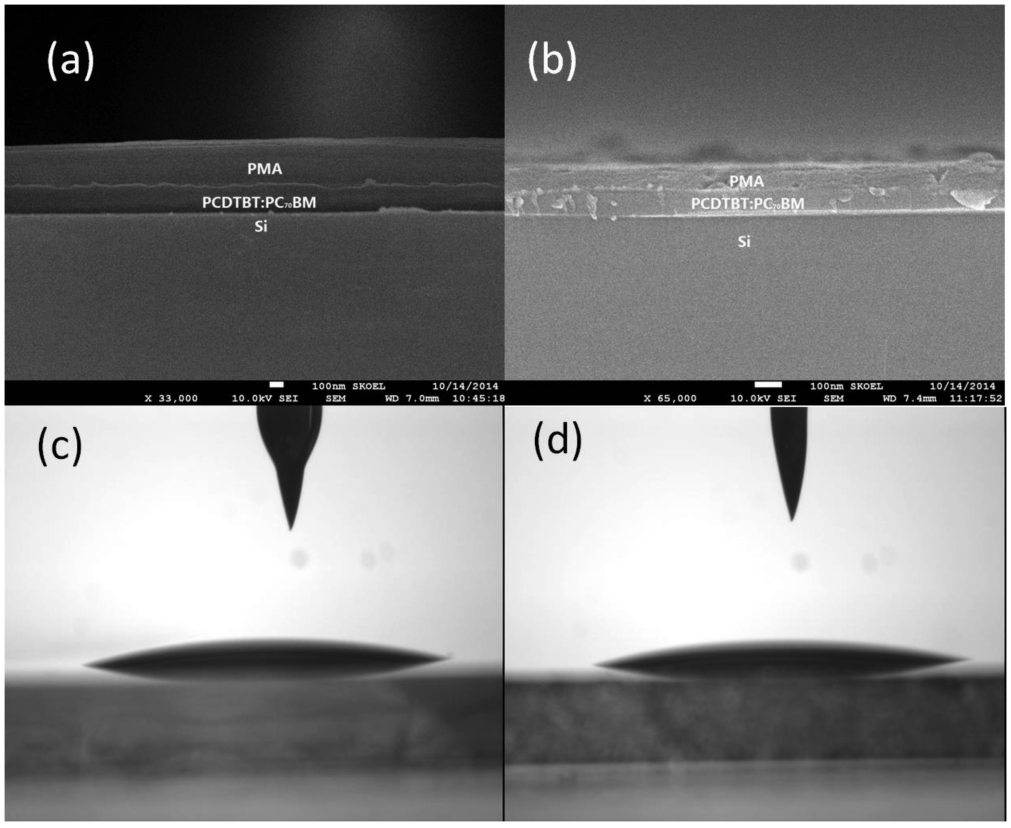

Figure 5. Cross-sectional SEM images of the device except Ag anode (a) without modification by isopropyl alcohol and (b) modification by isopropyl alcohol. The contact angle of the PMA solution on the surface of active layer (c) without modification by isopropyl alcohol and (d) modification by isopropyl alcohol.

DOI: 10.1021/am508828n
ACS Appl. Mater. Interfaces 2015, 7, 5367–5372

the adhesion of active layer and results in reduced series resistance. As the solvent of PMA solution is also IPA, which is used for surface modification, it also functioned as a surfactant to reduce the surface tension of PMA liquids. From the Young equation[43]

$$\cos\theta_c = \frac{\gamma_{SV} - \gamma_{SL}}{\gamma}$$

it is clear that the contact angle (θ_c) of a droplet strongly depends on its surface tension γ, on the assumption that the solid−vapor phase (γ_{SV}) and the solid−liquid phase (γ_{SL}) interactions are fixed. Therefore, a large surface tension implies a large contact angle. The smaller the contact angle is, the less volume of liquid is needed to fully cover the substrate, and the more uniform the whole film surface. Improved adhesion also leads to perfect interface contact between the active layer and the PMA solution, which results in enhanced hole transport to the Ag electrode and thus improved PCE.

To optimize the device performance, we fabricated devices with different PMA concentrations of 1, 2.5, 5, and 10 mg/mL. All the PMA solutions were spin-coated at the speed of 4000 r/min for 30 s after the pretreatment using IPA. For comparison, the device without HTL was fabricated as the control device. The $J-V$ characteristics of all the devices are shown in Figure 6a. As can be seen, devices with PMA HTL outperformed the

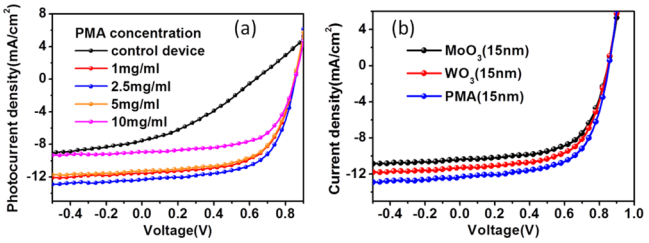

Figure 6. $J-V$ characteristics of devices (a) without PMA, with 1, 2.5, 5, and 10 mg/mL PMA and (b) with MoO_3, WO_3, and PMA as HTL.

control device in all the photovoltaic parameters. The control device has the poor performance, including an open-circuit voltage (V_{oc}) of 0.63 V, a short-circuit current (J_{sc}) of 8.32 mA/cm^2, and an FF value of 33.3%. This leads to a lower PCE of only 1.75%. Amazingly, after the pretreatment using IPA, the device with 2.5 mg/mL PMA shows the best PCE of 6.57%, with a V_{oc} of 0.85 V, a J_{sc} of 12.5 mA/cm^2, and an FF of 61.8%. All the photovoltaic parameters are summarized in Table 1, and the corresponding thickness of PMA layers with different concentrations are also measured. Other materials (MoO_3, WO_3) are used as HTL to compare the performance, and the results are shown in Figure 7b. It can be seen that the device performance with MoO_3 and WO_3 as HTL is a little lower than that of device with PMA. It can be attributed to the better

Table 1. Photovoltaic Parameters of Devices with Different Concentrations of PMA

device types	PMA thickness (nm)	J_{sc} (mA/cm^2)	V_{oc} (V)	FF (%)	PCE (%)
control	0	8.32	0.63	33.3	1.75
1 mg/mL	8	11.4	0.85	61.5	5.96
2.5 mg/mL	15	12.5	0.85	61.8	6.57
5 mg/mL	20	11.5	0.85	61.6	6.02
10 mg/mL	38	9.0	0.85	61.4	4.70

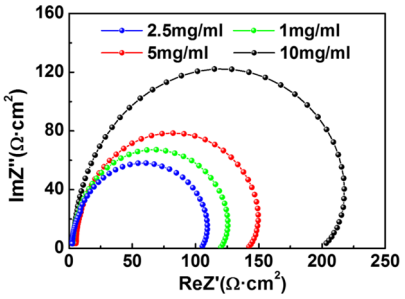

Figure 7. Complex impedance spectra of the devices with different concentrations.

interface contact between active layer and electrode. It is easy to understand that the performance improvement comes from perfect hole transporting and electron blocking by PMA layer in electrical aspect. In this comparison condition, there exist two kinds of interfaces containing active layer/metal and active layer/PMA/metal. The direct contact between the metal and active layers will result in local serious shunt loss and consequently lead to reduced V_{oc}, J_{sc}, and FF.[44,45] To obtain additional information about the interfacial characteristics of PMA in these devices, impedance spectroscopy was measured with an alternating current signal of 1 V in the frequency range of 20 Hz−1 MHz. The complex impedance spectra of the devices with different concentrations of PMA are shown in Figure 7. Three columns of data were obtained, which are frequency (Hz), impedance, and angle, respectively. The data of x-axis are obtained with the formula of impedance × cos(angle/180π), which refers to the real part of the complex impedance, while the data of y-axis are obtained with the formula of impedance × sin(angle/180π), which refers to the imaginary part of the complex impedance. The shapes of impedance spectra are both semicircles that are beneficial to investigate the interface resistance in PSCs. The series resistance of devices is related to the diameters of the semicircles. It can be seen that impedance spectroscopy of device with 2.5 mg/mL PMA shows the smallest diameter, which indicates the smallest series resistance. The diameter of impedance spectroscopy increases along with the increase of PMA concentration. This phenomenon is consistent with the measured photocurrent and total solar-to-power conversion efficiency of the four devices in the order of 2.5 > 1 > 5 >10 mg/mL.

In optical aspect, it is noticed that absorption of light of wavelength range of 400−500 nm is not as low as ideal and that this absorption is nonignorable. Therefore, to determine whether the cells built with the higher concentrations show a decreased J_{sc} simply because the thicker PMA layer absorbs more light, which should be reflected into active layer for the second round absorption, we conducted a simulation of the current density on dependence of the thickness of the PMA layer, which is shown in Figure 8. The simulation is based on the transfer matrix method (TMM)[46,47] on the assumption that the internal quantum efficiency is 100%. The optical constants of PMA are obtained by spectroscopic ellipsometry. It can be seen clearly that the current density varies with the change of the PMA layer thickness and reaches a maximum when the thickness of PMA layer is ∼13 nm. All the PMA solutions with different concentrations used in our devices were spin-coated at a fixed speed of 4000 r/min. This means that the thickness of PMA is increased with the improved PMA solution concentration, so the thickness of PMA layer is in direct

DOI: 10.1021/am508828n
ACS Appl. Mater. Interfaces 2015, 7, 5367−5372

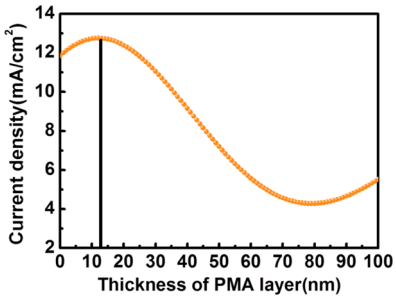

Figure 8. Optical simulated current density characteristics with different thicknesses of PMA layer.

proportion to the PMA solution concentration. Therefore, the cells built with the higher concentrations show a decreased J_{sc} simply because the thicker PMA layer absorbs more light.

Figure 9 shows the IPCE spectra of devices with different concentrations of PMA, where the IPCE values for each

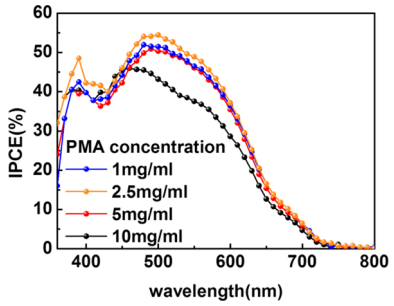

Figure 9. IPCE spectra of devices with different concentrations of PMA in the wavelength range from 350 to 800 nm.

wavelength from 300 to 800 nm are plotted as a function of wavelength. Owing to a stronger hole extraction capability of PMA, the IPCE of the four devices is much higher than that of the control device. The IPCE of device with 2.5 mg/mL PMA outperformed than the rest of the devices in the wavelength range from 450 to 600 nm.

CONCLUSION

In summary, we present a facile way of polymer solar cell fabrication by using the solution-processed PMA as an efficient HTL without any postannealing. The PMA powder was dissolved in IPA and then spin-coated onto the active layer right after a pretreatment by IPA. The IPA-treatment procedure further decreases the contact angle and smoothes the interfaces, which results in an improvement in the performance of the device. The optimum concentration of PMA is 2.5 mg/mL, and our device achieved an improved PCE of 6.57%. The annealing-free HTL makes it more promising for large-scale production of organic solar cells.

AUTHOR INFORMATION

Corresponding Authors

*E-mail: shenliang@jlu.edu.cn. (L.S.)
*E-mail: ruansp@jlu.edu.cn. (S.R.)

Notes

The authors declare no competing financial interest.

ACKNOWLEDGMENTS

The authors are grateful to National Natural Science Foundation of China (Grant Nos. 61275035, 61370046, and 51303061), Project of Science and Technology Development Plan of Jilin Province (Grant Nos. 20110314 and 20130206021GX), Scientific Frontier and Interdiscipline Innovative Projects of Jilin University (Grant No. 2013ZY18), Key Technology Research and Development Program of Changchun (No.13KG66), and Graduate Innovation Fund of Jilin University (Grant No. 2014021).

REFERENCES

(1) Lessard, B. H.; Dang, J. D.; Grant, T. M.; Gao, D.; Seferos, D. S.; Bender, T. P. Bis(Tri-*N*-Hexylsilyl Oxide) Silicon Phthalocyanine: A Unique Additive in Ternary Bulk Heterojunction Organic Photovoltaic Devices. *ACS Appl. Mater. Interfaces.* **2014**, *6*, 15040−15051.
(2) Walker, B.; Han, X.; Kim, C.; Sellinger, A.; Nguyen, T. Q. Solution-Processed Organic Solar Cells from Dye Molecules: An Investigation of Diketopyrrolopyrrole:Vinazene Heterojunctions. *ACS Appl. Mater. Interfaces.* **2012**, *4*, 244−250.
(3) Li, Y. Molecular Design of Photovoltaic Materials for Polymer Solar Cells: Toward Suitable Electronic Energy Levels and Broad Absorption. *Acc. Chem. Res.* **2012**, *45*, 723−733.
(4) Park, B.; Yun, S. H.; Cho, C. Y.; Kim, Y. C.; Shin, J. C.; Jeon, H. G.; Huh, Y. H.; Hwang, I.; Baik, K. Y.; Lee, Y. I.; Uhm, H. S.; Cho, G. S.; Choi, E. H. Surface Plasmon Excitation in Semitransparent Inverted Polymer Photovoltaic Devices and Their Applications as Label-Free Optical Sensors. *Light: Sci. Appl.* **2014**, *3*, e222.
(5) Angmo, D.; Gevorgyan, S. A.; Larsen-Olsen, T. T.; Søndergaard, R. R.; Hösel, M.; Jørgensen, M.; Gupta, R.; Kulkarni, G. U.; Krebs, F. C. Scalability and Stability of Very Thin, Roll-to-Roll Processed, Large Area, Indium-Tin-Oxide Free Polymer Solar Cell Modules. *Org. Electron.* **2013**, *14*, 984−994.
(6) Mishra, A.; Bauerle, P. Small Molecule Organic Semiconductors on the Move: Promises for Future Solar Energy Technology. *Angew. Chem., Int. Ed. Engl.* **2012**, *51*, 2020−2067.
(7) He, Z.; Zhong, C.; Huang, X.; Wong, W. Y.; Wu, H.; Chen, L.; Su, S.; Cao, Y. Simultaneous Enhancement of Open-Circuit Voltage, Short-Circuit Current Density, and Fill Factor in Polymer Solar Cells. *Adv. Mater.* **2011**, *23*, 4636−4643.
(8) Zhang, S.; Ye, L.; Zhao, W.; Yang, B.; Wang, Q.; Hou, J. Realizing over 10% Efficiency in Polymer Solar Cell by Device Optimization. *Sci. China. Chem.* **2015**, *58*, 248−256.
(9) Liu, Y.; Zhao, J.; Li, Z.; Mu, C.; Ma, W.; Hu, H.; Jiang, K.; Lin, H.; Ade, H.; Yan, H. Aggregation and Morphology Control Enables Multiple Cases of High-Efficiency Polymer Solar Cells. *Nat.Commun.* **2014**, *5*, 5293.
(10) Chen, J. D.; Cui, C.; Li, Y. Q.; Zhou, L.; Ou, Q. D.; Li, C.; Li, Y.; Tang, J. X. Single-Junction Polymer Solar Cells Exceeding 10% Power Conversion Efficiency. *Adv. Mater.* **2015**, *27*, 1035−1041.
(11) Stratakis, E.; Kymakis, E. Nanoparticle-Based Plasmonic Organic Photovoltaic Devices. *Mater. Today.* **2013**, *16*, 133−146.
(12) Kouijzer, S.; Esiner, S.; Frijters, C. H.; Turbiez, M.; Wienk, M. M.; Janssen, R. A. J. Efficient Inverted Tandem Polymer Solar Cells with a Solution-Processed Recombination Layer. *Adv. Energy Mater.* **2012**, *2*, 945−949.
(13) Sun, Y.; Takacs, C. J.; Cowan, S. R.; Seo, J. H.; Gong, X.; Roy, A.; Heeger, A. J. Efficient, Air-Stable Bulk Heterojunction Polymer Solar Cells Using MoO(X) as the Anode Interfacial Layer. *Adv. Mater.* **2011**, *23*, 2226−2230.
(14) Zhang, Z.-G.; Qi, B.; Jin, Z.; Chi, D.; Qi, Z.; Li, Y.; Wang, J. Perylene Diimides: A Thickness-Insensitive Cathode Interlayer for High Performance Polymer Solar Cells. *Energy Environ. Sci.* **2014**, *7*, 1966.
(15) Tan, Z.; Li, L.; Wang, F.; Xu, Q.; Li, S.; Sun, G.; Tu, X.; Hou, X.; Hou, J.; Li, Y. Solution-Processed Rhenium Oxide: A Versatile Anode

DOI: 10.1021/am508828n
ACS Appl. Mater. Interfaces 2015, 7, 5367−5372

Buffer Layer for High Performance Polymer Solar Cells with Enhanced Light Harvest. *Adv. Energy Mater.* **2014**, *4*, 1300884.
(16) Tan, Z.; Zhang, W.; Zhang, Z.; Qian, D.; Huang, Y.; Hou, J.; Li, Y. High-Performance Inverted Polymer Solar Cells with Solution-Processed Titanium Chelate as Electron-Collecting Layer on ITO Electrode. *Adv. Mater.* **2012**, *24*, 1476−1481.
(17) Choi, H.; Park, J. S.; Jeong, E.; Kim, G. H.; Lee, B. R.; Kim, S. O.; Song, M. H.; Woo, H. Y.; Kim, J. Y. Combination of Titanium Oxide and a Conjugated Polyelectrolyte for High-Performance Inverted-Type Organic Optoelectronic Devices. *Adv. Mater.* **2011**, *23*, 2759−2763.
(18) Lee, S. J.; Pil Kim, H.; Mohd Yusoff, A. R. b.; Jang, J. Organic Photovoltaic with PEDOT:PSS and V_2O_5Mixture as Hole Transport Layer. *Sol. Energy Mater. Sol. Cells* **2014**, *120*, 238−243.
(19) Zhang, Y.; Yuan, S.; Liu, W. Inverted Organic Solar Cells Employing RGO/TiOx Composite Films as Electron Transport Layers. *Electrochim. Acta* **2014**, *143*, 18−22.
(20) Chen, L.-M.; Xu, Z.; Hong, Z.; Yang, Y. Interface Investigation and Engineering—Achieving High Performance Polymer Photovoltaic Devices. *J. Mater. Chem.* **2010**, *20*, 2575.
(21) Chen, S.; Manders, J. R.; Tsang, S.-W.; So, F. Metal Oxides for Interface Engineering in Polymer Solar Cells. *J. Mater. Chem.* **2012**, *22*, 24202.
(22) Ratcliff, E. L.; Zacher, B.; Armstrong, N. R. Selective Interlayers and Contacts in Organic Photovoltaic Cells. *J. Phys. Chem. Lett.* **2011**, *2*, 1337−1350.
(23) Yip, H.-L.; Jen, A. K. Y. Recent Advances in Solution-Processed Interfacial Materials for Efficient and Stable Polymer Solar Cells. *Energy. Environ. Sci.* **2012**, *5*, 5994.
(24) Cao, H.; He, W.; Mao, Y.; Lin, X.; Ishikawa, K.; Dickerson, J. H.; Hess, W. P. Recent Progress in Degradation and Stabilization of Organic Solar Cells. *J. Power Sources* **2014**, *264*, 168−183.
(25) Lee, H.-M.; Noh, Y.-J.; Na, S.-I.; Chung, K.-B.; Kim, H.-K. PEDOT:PSS-Free Organic Solar Cells Fabricated on Buffer and Anode Integrated Ta-Doped In_2O_3 Films. *Sol. Energy Mater. Sol. Cells* **2014**, *125*, 145−154.
(26) Garcia, A.; Welch, G. C.; Ratcliff, E. L.; Ginley, D. S.; Bazan, G. C.; Olson, D. C. Improvement of Interfacial Contacts for New Small-Molecule Bulk-Heterojunction Organic Photovoltaics. *Adv. Mater.* **2012**, *24*, 5368−5373.
(27) Xiang, C.; Koo, W.; So, F.; Sasabe, H.; Kido, J. A Systematic Study on Efficiency Enhancements in Phosphorescent Green, Red and Blue Microcavity Organic Light Emitting Devices. *Light: Sci. Appl.* **2013**, *2*, e74.
(28) Kohlstädt, M.; Grein, M.; Reinecke, P.; Kroyer, T.; Zimmermann, B.; Würfel, U. Inverted Ito- and Pedot:Pss-Free Polymer Solar Cells with High Power Conversion Efficiency. *Sol. Energy Mater. Sol. Cells* **2013**, *117*, 98−102.
(29) Palilis, L. C.; Vasilopoulou, M.; Douvas, A. M.; Georgiadou, D. G.; Kennou, S.; Stathopoulos, N. A.; Constantoudis, V.; Argitis, P. Solution Processable Tungsten Polyoxometalate as Highly Effective Cathode Interlayer for Improved Efficiency and Stability Polymer Solar Cells. *Sol. Energy Mater. Sol. Cells* **2013**, *114*, 205−213.
(30) Wang, F.; Tan, Z.; Li, Y. Solution-Processable Metal Oxides/Chelates as Electrode Buffer Layers for Efficient and Stable Polymer Solar Cells. *Energy Environ. Sci.* **2014**, DOI: 10.1039/C4EE03802A.
(31) Tan, Z.; Li, L.; Cui, C.; Ding, Y.; Xu, Q.; Li, S.; Qian, D.; Li, Y. Solution-Processed Tungsten Oxide as an Effective Anode Buffer Layer for High-Performance Polymer Solar Cells. *J. Phys. Chem.C* **2012**, *116*, 18626−18632.
(32) Zeng, W.; Yong, K. S.; Kam, Z. M.; Chen, Z.-k.; Li, Y. Effect of Moo3 as an Interlayer on the Performance of Organic Solar Cells Based on Znpc and C_{60}. *Synth. Met.* **2012**, *161*, 2748−2752.
(33) Qin, P.; Fang, G.; Cheng, F.; Ke, W.; Lei, H.; Wang, H.; Zhao, X. Sulfur-Doped Molybdenum Oxide Anode Interface Layer for Organic Solar Cell Application. *ACS Appl. Mater. Interfaces* **2014**, *6*, 2963−2973.
(34) Girotto, C.; Voroshazi, E.; Cheyns, D.; Heremans, P.; Rand, B. P. Solution-Processed MoO(3) Thin Films as a Hole-Injection Layer for Organic Solar Cells. *ACS Appl. Mater. Interfaces* **2011**, *3*, 3244−3247.
(35) Tan, Z.; Qian, D.; Zhang, W.; Li, L.; Ding, Y.; Xu, Q.; Wang, F.; Li, Y. Efficient and Stable Polymer Solar Cells with Solution-Processed Molybdenum Oxide Interfacial Layer. *J. Mater. Chem. A* **2013**, *1*, 657.
(36) Cho, S.-P.; Yeo, J.-S.; Kim, D.-Y.; Na, S.-i.; Kim, S.-S. Brush Painted V_2O_5 Hole Transport Layer for Efficient and Air-Stable Polymer Solar Cells. *Sol. Energy Mater. Sol. Cells* **2015**, *132*, 196−203.
(37) Shelton, S. W.; Chen, T. L.; Barclay, D. E.; Ma, B. Solution-Processable Triindoles as Hole Selective Materials in Organic Solar Cells. *ACS Appl. Mater. Interfaces* **2012**, *4*, 2534−2540.
(38) Tan, Z.; Zhang, W.; Cui, C.; Ding, Y.; Qian, D.; Xu, Q.; Li, L.; Li, S.; Li, Y. Solution-Processed Vanadium Oxide as a Hole Collection Layer on an ITO Electrode for High-Performance Polymer Solar Cells. *Phys. Chem. Chem. Phys.* **2012**, *14*, 14589−14595.
(39) Zhu, Y.; Yuan, Z.; Cui, W.; Wu, Z.; Sun, Q.; Wang, S.; Kang, Z.; Sun, B. A Cost-Effective Commercial Soluble Oxide Cluster for Highly Efficient and Stable Organic Solar Cells. *J. Mater. Chem. A* **2014**, *2*, 1436.
(40) Long, D. L.; Burkholder, E.; Cronin, L. Polyoxometalate Clusters, Nanostructures and Materials: From Self Assembly to Designer Materials and Devices. *Chem. Soc. Rev.* **2007**, *36*, 105−121.
(41) Shen, L.; Xu, Y.; Zhang, X.; Meng, F.; Ruan, S.; Chen, W. Short-Circuit Current Density Improvement of Inverted Polymer Solar Cells Using Pbpc to Enhance Photon Absorption over 600 nm. *Sol. Energy Mater. Sol. Cells* **2010**, *94*, 2451−2454.
(42) Yu, W.; Shen, L.; Ruan, S.; Meng, F.; Wang, J.; Zhang, E.; Chen, W. Performance Improvement of Inverted Polymer Solar Cells Thermally Evaporating Nickel Oxide as an Anode Buffer Layer. *Sol. Energy Mater. Sol. Cells* **2012**, *98*, 212−215.
(43) Girotto, C.; Moia, D.; Rand, B. P.; Heremans, P. High-Performance Organic Solar Cells with Spray-Coated Hole-Transport and Active Layers. *Adv. Funct. Mater.* **2011**, *21*, 64−72.
(44) Liao, Y.-K.; Kuo, S.-Y.; Hsieh, M.-Y.; Lai, F.-I.; Kao, M.-H.; Cheng, S.-J.; Chiou, D.-W.; Hsieh, T.-P.; Kuo, H.-C. A Look into the Origin of Shunt Leakage Current of Cu(in,Ga)Se2 Solar Cells Via Experimental and Simulation Methods. *Sol. Energy Mater. Sol. Cells* **2013**, *117*, 145−151.
(45) Shao, S.; Liu, J.; Bergqvist, J.; Shi, S.; Veit, C.; Würfel, U.; Xie, Z.; Zhang, F. In Situ Formation of MoO_3 in PEDOT:PSS Matrix: A Facile Way to Produce a Smooth and Less Hygroscopic Hole Transport Layer for Highly Stable Polymer Bulk Heterojunction Solar Cells. *Adv. Energy. Mater.* **2013**, *3*, 349−355.
(46) Holman, Z. C.; De Wolf, S.; Ballif, C. Improving Metal Reflectors by Suppressing Surface Plasmon Polaritons: A Priori Calculation of the Internal Reflectance of a Solar Cell. *Light: Sci. Appl.* **2013**, *2*, e106.
(47) Lee, K.-T.; Lee, J. Y.; Seo, S.; Guo, L. J. Colored Ultrathin Hybrid Photovoltaics with High Quantum Efficiency. *Light: Sci. Appl.* **2014**, *3*, e215.

DOI: 10.1021/am508828n
ACS Appl. Mater. Interfaces 2015, 7, 5367−5372